REPORT DOCUMENTATION PAGE

AFRL-SR-BL-TR-01-

0620

1. REPORT DATE (DD-MM-YYYY)	2. REPORT TYPE	3. DATES COVERED (From - To)
13-11-2001	Final Performance Report	12/1/99-11/30/00

4. TITLE AND SUBTITLE

Visual navigation and space perception

5a. CONTRACT NUMBER
F4620-98-1-0337

5b. GRANT NUMBER

5c. PROGRAM ELEMENT NUMBER
61102F

6. AUTHOR(S)
Martin S. Banks

5d. PROJECT NUMBER
2313

5e. TASK NUMBER
~~CX~~ BX

5f. WORK UNIT NUMBER

7. PERFORMING ORGANIZATION NAME(S) AND ADDRESS(ES)
School of Optometry, 360 Minor, Univ of Calif, Berkeley

Berkeley, CA 94720-2020

8. PERFORMING ORGANIZATION REPORT NUMBER

9. SPONSORING / MONITORING AGENCY NAME(S) AND ADDRESS(ES)

12. DISTRIBUTION / AVAILABILITY STATEMENT

13. SUPPLEMENTARY NOTES

14. ABSTRACT The problem of visual space perception is the recovery of the location, shape, size, and orientation of objects in the environment from the pattern of light reaching the eyes. Similarly, the problem of visual navigation is the recovery of an observer's self-motion with respect to the environment from the moving pattern of light reaching the eyes and the complex of extra-retinal signals including eye-muscle, neck-muscle, and vestibular signals. During the last two and a half years, we continued our theoretical and experimental investigations of human visual navigation and space perception. Our accomplishments include several publications in referred scientific journals, the completion of a rotating chair apparatus for use in studying visual-vestibular interactions, and the development of numerous software tools for the control of psychophysical experimentation including graphic display, control of external devices, and analysis of experimental data. These accomplishments are relevant to several aspects of the military aviation mission including 1) how the use of synthetic visual displays (virtual reality in the advanced cockpit, night-vision goggles, etc.) will affect perceived self-motion and spatial orientation, 2) how extra-retinal signals that occur in high-performance flying will affect perceived self-motion and orientation and 3) what visual properties synthetic displays will have to have to prevent or minimize spatial disorientation illusions.

15. SUBJECT TERMS

16. SECURITY CLASSIFICATION OF:			17. LIMITATION OF ABSTRACT	18. NUMBER OF PAGES	19a. NAME OF RESPONSIBLE PERSON
a. REPORT	b. ABSTRACT	c. THIS PAGE		21	Martin S. Banks
					19b. TELEPHONE NUMBER (include area code) 510-642-9341

Final Technical Report
F49620-98-1-0337

Visual Navigation and Space Perception

Martin S. Banks
School of Optometry and Vision Science Program
University of California, Berkeley

Technical Report
Visual Navigation & Space Perception
M.S. Banks

During the last two and a half years, we worked on three general problems: Surface perception, heading perception, and visual-haptic integration. In this progress report, we review the work leading up to our current work (thus some of the material appeared on last year's progress report) and then we discuss the work completed this past year.

1. Surface Perception

The problem of visual space perception is the recovery of the location, shape, size, and orientation of objects in the environment from the pattern of light reaching the eyes. The visual system uses disparities between the two retinal images to glean information about the 3-D layout of the environment. In the last seven years, we have investigated how disparity is used to recover surface orientation. Most of the work has concerned determining the slant of an isolated surface rotated about a vertical axis. This problem is interesting because the pattern of disparities depends not only on slant, but also on location relative to the head (Ogle, 1950).

The first part of this section is basically the same as last year's progress report because we need to explain the background to the work we accomplished during the two and a half year grant period. If you have already read this background material from previous progress reports, you can skip ahead to page 5.

Figure 1.1 depicts the geometry for binocular viewing of a vertical plane. The objective gaze-normal surface is the plane perpendicular to the cyclopean line of sight. The slant S is the angle by which the plane of interest is rotated about a vertical axis from the gaze-normal surface.

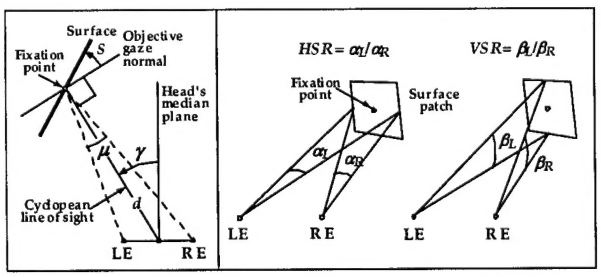

Figure 1.1. Binocular viewing geometry. See text.

What signals are available for slant estimation? One important signal is horizontal disparity. For a smooth surface slanted about a vertical axis, the horizontal disparity pattern can be represented locally by the horizontal size ratio (*HSR*; Figure 1.1), the ratio of horizontal angles the patch subtends in the left and right eyes (Rogers & Bradshaw, 1993). Changes in *HSR* produce obvious and immediate changes in perceived slant, so this signal must be involved in slant estimation. However, *HSR* by itself is ambiguous. To illustrate the ambiguity, Figure 1.2 shows several surface patches that give rise to *HSR*s of 1 and 1.04. For each *HSR* value, there is an infinitude of possible slants depending on the surface's location. Clearly, the measurement of *HSR* alone does not allow an unambiguous estimate of the surface's orientation nor do any other descriptions of horizontal disparity (Longuet-Higgins, 1982). A main purpose of our work has been to determine what other signals are used, in combination with horizontal disparity, by the visual system and to determine how those signals are combined to determine surface slant.

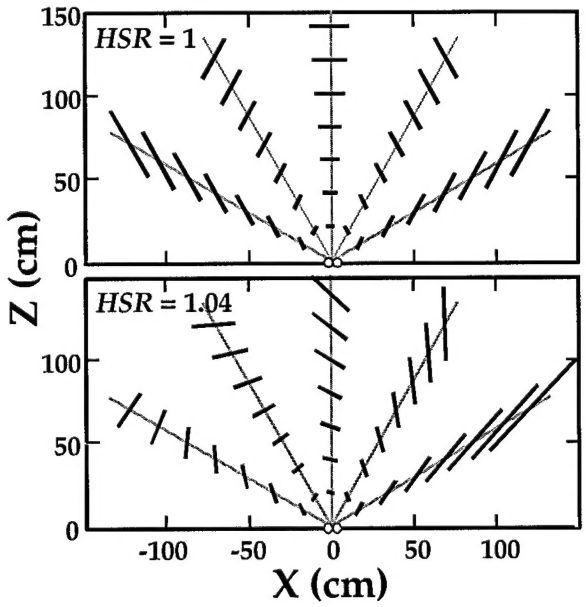

Figure 1.2. Ambiguity of *HSR*. Plan view with the abscissa representing lateral position and the ordinate forward position. The line segments represent surface patches that give rise to *HSR* = 1 (upper panel) and *HSR* = 1.04 (lower panel).

Another potentially useful signal is vertical disparity which can be represented by the vertical size ratio (*VSR*; Figure 1.1), the ratio of vertical angles subtended by a surface patch in the left and right eyes. *VSR* varies with the location of a surface patch relative to the head, but does not vary with surface slant (Gillam &

Lawergren, 1983). The circles in Figure 1.3 show the *VSR* at various locations in the visual plane. Another signal is the rate of change in *VSR* with azimuth ($\partial VSR/\partial\gamma$); this signal depends strongly on distance and less so on slant.

Other useful signals are provided by sensed eye position. Ignoring torsion, each eye has one degree of freedom in the visual plane. We can thus represent binocular eye position by two values, γ and μ, the version and vergence of the eyes (Figure 1.1).

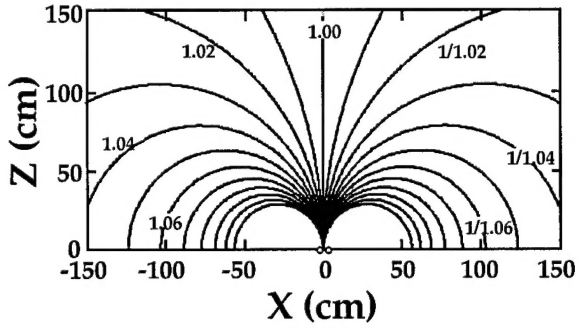

Figure 1.3. Iso*VSR* contours. Plan view. Abscissa represents lateral position and ordinate forward position. Each contour represents the regions in space for which *VSR* is constant; each contour represents a different *VSR*.

Finally, useful slant information can be gleaned from nonstereoscopic signals such as the texture gradient created by projection onto the retinae of surfaces with statistically regular textures (Cutting & Millard, 1984; Buckley & Frisby, 1993; Cumming et al, 1993). Such cues were present in older stereoscopic work using real objects (e.g., Ogle, 1938; Gillam et al, 1988). In more recent work with computer displays, there is still generally a perspective cue that indicates that the surface is frontoparallel to the head (e.g., Rogers & Bradshaw, 1995; Howard & Kaneko, 1994). Neither the slant specified by a given texture gradient nor the uncertainty of the estimation varies with distance or azimuth (Sedgwick, 1986; Backus et al, 1999).

An unambiguous estimate of slant can be obtained from various combinations of the above-mentioned signals. For example, slant can in principle be estimated from *HSR* and sensed eye position (Ogle, 1950; Foley, 1980). From Backus et al (1999):

$$\hat{S} \approx -\tan^{-1}\left(\frac{1}{\mu}\ln HSR - \tan\gamma\right). \qquad (1.1)$$

The estimates of μ and γ ($\hat{\mu}$ and $\hat{\gamma}$) are presumably derived from extra-retinal, eye-position signals. Correcting *HSR* via eye position has the important consequence of compensating for the changes in binocular viewing geometry that occur with changes in distance and azimuth (Kaneko & Howard, 1996; Ogle, 1950).

Slant can also be estimated from retinal-image information alone (Gårding, *et al.*, 1995; Gillam & Lawergren, 1983; Koenderink & van Doorn, 1976; Mayhew & Longuet-Higgins, 1982). From Backus et al:

$$\hat{S} \approx -\tan^{-1}\left(\frac{1}{\mu}\ln\frac{HSR}{VSR}\right) \qquad (1.2)$$

where μ can be measured from retinal image properties alone. In the terminology of Gårding et al (1995), μ "normalizes" the slant (scales *HSR* for changes due to viewing distance) and *VSR* "corrects" the slant (corrects *HSR* for changes due to azimuth).

In summary, certain subsets of signals allow unambiguous estimation of slant and we can summarize them with three calculations (Banks & Backus, 1998a): (1) slant estimation from *HSR* and eye position ($\hat{S}_{HSR,EP}$), (2) slant estimation from *HSR* and *VSR* ($\hat{S}_{HSR,VSR}$), and (3) slant estimation from nonstereoscopic cues such as perspective ($\hat{S}_P$).

In natural viewing, the slant estimates derived from these three methods should on average agree. However, each signal measurement is subject to error, so even in natural viewing, the estimates will differ. Because a surface can only have one slant at a time, the visual system must derive one estimate from the set of somewhat discrepant signals. In our conceptualization, the weight associated with each slant estimate is a function of its estimated reliability, and the estimated reliability is based in turn on the quality of the information present in the signals (e.g., Landy et al., 1995; Heller & Trahiotis, 1996). Several factors influence signal reliability. For example, consider the effects of increasing viewing distance. As distance increases, there is no effect on the information carried by the perspective signal (assuming broadband texture; Sedgwick, 1986), but the information carried by *HSR* is reduced because a given set of slants maps onto ever smaller ranges of *HSR*. Consequently, nonstereoscopic slant estimates should be weighted more heavily relative to stereoscopic slant estimates as viewing distance increases; experimental evidence confirms this expectation (Buckley & Frisby, 1993; Backus & Banks, 1999).

Some of our experiments examined whether the signals described above are used in estimating slant, and how the weights assigned to the estimates vary across viewing conditions and stimulus properties.

To do these experiments, we built a haploscope that allows independent manipulation of eye position and disparity. We examined the use of the two stereoscopic means of slant estimation described above. (We made

nonstereo, perspective information uninformative by using a "back projection" procedure; Banks & Backus, 1998a.) Observers rotated a stereoscopic random-dot plane about a vertical axis until it appeared normal to the line of sight: that is, they adjusted its slant until it was apparently gaze normal. Real and simulated versions were varied from 15° to the left of head-centric straight ahead to 15° to the right. Real version was varied by turning the haploscope arms so that the observer rotated the eyes to the desired version position. Simulated version was varied by altering the disparity field. Thus, an observer might look at a stereo plane with eyes rotated leftward while the disparities presented were as if the eyes were rotated rightward. If the visual system relies on extra-retinal, eye-position signals ($\hat{S}_{HSR,EP}$, slant estimation by *HSR* and eye position) in estimating the slant of a stereoscopic surface, then the observers' settings would be predicted from their actual eye positions; these predictions are represented by the diagonal line in the left panel of Figure 1.4. If, on the other hand, the system uses the information contained in the disparity field alone ($\hat{S}_{HSR,VSR}$, estimation by *HSR* and *VSR*), the settings would be predicted by the simulated eye positions; these predictions are represented by the three horizontal lines (one for each of three simulated eccentricities) in the left panel of Figure 1.4.

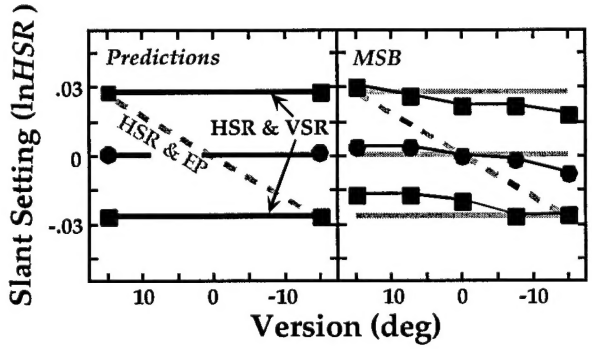

Figure 1.4. Predictions and results, Backus et al (1999). Natural log of *HSR* settings is plotted as a function of version. Left panel: Predictions. Slant estimation by *HSR* and eye position predicts the diagonal line. Estimation by *HSR and VSR* predicts the three horizontal lines (one for each *VSR*). Right panel: Results from one of 3 observers. Squares, circles, and squares represent results with different *VSR* values.

The results are displayed in the right panel of Figure 1.4. The data agree quite well with the predictions of $\hat{S}_{HSR,VSR}$. The actual version of the eyes had no clear effect on slant settings which is counter to the predictions of $\hat{S}_{HSR,EP}$. Thus, with large targets, compensation for eccentric viewing is based primarily on the pattern of horizontal and vertical disparities within the images and little on actual eye position. We can summarize these findings by expressing the slant estimates as weighted averages of the signals presented to the visual system: $\hat{S} = w_{H,V}\hat{S}_{HSR,VSR} + w_{H,E}\hat{S}_{HSR,EP}$ where the w's represent the associated weights. We can ignore the nonstereo slant estimator in this experiment (not expressed in equation) because it always specified a slant of 0 and thereby could have no influence in a slant-nulling task. The data in Figure 1.4 can be fit well by this model if $w_{H,V}$=.85 and $w_{H,E}$=.15.

The magnitudes of vertical disparities at a given azimuth are roughly proportional to elevation above the visual plane (*VSR* is, however, constant in the Fick coordinates we use for our equations). Thus, surfaces that subtend a small vertical angle do not create large vertical disparities. We took advantage of this by reducing stimulus height.

The results for one observer are shown in Figure 1.5. Stimulus width was always 40°, but the height varied from 0–30° (left to right in the figure). When the height was 30°, we again found that slant settings were determined almost exclusively by $\hat{S}_{HSR,VSR}$. However, as stimulus height was reduced, the slant settings became more and more consistent with $\hat{S}_{HSR,EP}$. Finally, with a stimulus height of 0° (horizontal row of dots), slant settings were predicted entirely by $\hat{S}_{HSR,EP}$; thus, as the eyes turned, different patterns of disparity were required for a gaze-normal percept.

These results show clearly that the human visual system employs two means of estimating slant of stereoscopically defined surfaces. The weight given $\hat{S}_{HSR,VSR}$ is high when the stimulus is large and contains measurable vertical disparities. The weight given $\hat{S}_{HSR,EP}$ is high when the stimulus is short and does not contain readily measurable vertical disparities.

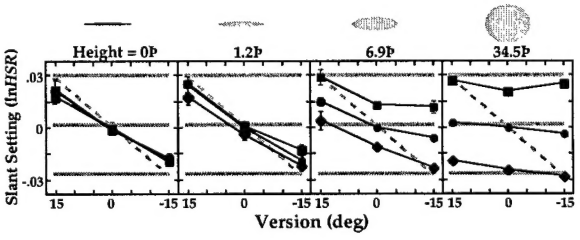

Figure 1.5. Slant settings for different stimulus heights. Natural log of *HSR* is plotted in each panel as a function of version. Panels from left to right show data when stimulus height varied from 0–35°. Predictions (see Figure 4) are also shown for two means of slant estimation.

The work described above focused on estimation of surface slant about a vertical axis. Naturally, the visual system must estimate slant about any axis, not just the vertical. One can show that the slant and tilt of a smooth surface can be recovered locally from estimates of the slant component about the vertical axis (tilt = 0°) and the component about the horizontal axis (tilt = 90°) (Backus et al, 1999). Thus, we investigated slant estimation about the horizontal axis and applied what we learned to estimation about arbitrary axes. We completed a paper on this topic during the grant period (Banks, Hooge, & Backus, 2001), so we describe that work here.

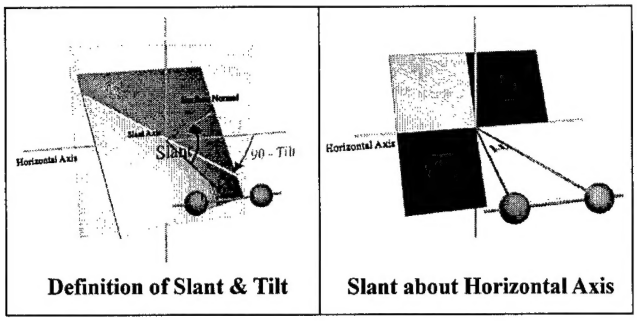

Figure 1.6. Binocular viewing geometry for estimating surface orientation. Left panel: Definitions of slant and tilt. A binocular observer is viewing a slanted plane. The cyclopean line of sight is represented by the line segment between the midpoint between the eyes and the fixation point, which is the center of the slanted plane. The large green plane is perpendicular to the cyclopean line of sight and represents the gaze-normal plane (for which slant = 0). The gray stimulus plane is rotated with respect to the gaze-normal plane. *Slant* is the angle between its surface normal and the cyclopean line of sight. *Tilt* is the angle between the horizontal meridian and the projection of the surface normal. *Slant axis* is the intersection of the gaze-normal plane and the stimulus plane and corresponds to the axis about which the stimulus plane is rotated relative to the normal plane. Right panel: Slant about a horizontal slant axis; tilt = 90 deg. The eyes are fixating the middle of the stimulus plane. The eyes' vergence (μ) is the angle between the lines of sight.

The horizontal disparity pattern associated with slant about a horizontal axis (right panel of Figure 1.6) can be represented locally as a horizontal-shear disparity. Ogle and Ellerbrock (1946) defined this disparity as follows. A line through the fixation point and perpendicular to the visual plane is a vertical line. There is a horizontal axis through the fixation point, in the visual plane, and parallel to the interocular axis. We rotate the vertical line about this axis and project the images of the line onto the two eyes. The horizontal-shear disparity (H_R) is the angle between the projections of the line in the two eyes. If the eyes are torsionally aligned (i.e., the horizontal meridians of the eyes are co-planar) and fixating in the head's median plane, slant about a horizontal axis is given by:

$$S = -\tan^{-1}\left[\frac{\tan(H_R/2)}{\sin(\tan^{-1}(i/2d))}\right] \qquad (1.3)$$

where S is the slant, i is the interocular distance, and d is the distance to the vertical line's midpoint. When the distance to the surface is much greater than the interocular distance, slant is given to close approximation by:

$$S \approx -\tan^{-1}\left(\frac{1}{\mu}\tan H_R\right) \qquad (1.4)$$

where μ is the eyes' horizontal vergence (right panel, Figure 1.6). Thus, estimating slant about a horizontal axis is straightforward when the eyes are aligned: the visual system must only measure the pattern of horizontal disparity (quantified by H_R) and the vergence distance (μ, which could also be measured by use of the pattern of vertical disparities; Rogers & Bradshaw, 1995; Backus et al., 1999).

The eyes, however, are not torsionally aligned in all viewing situations. Specifically, the eyes can rotate about the lines of sight; cyclovergence refers to rotations in opposite directions in the two eyes. Let τ represent cyclovergence in Helmholtz coordinates. Intortion ($\tau < 0$; tops of the eyeballs rotated toward one another) occurs with downward gaze at a near target and extorsion ($\tau > 0$) with upward gaze (Somani, DeSouza, Tweed, & Vilis, 1998). Figure 1.7 illustrates how the resulting torsional misalignment alters the horizontal disparities at the retinas. In each panel, there is a horizontal-shear disparity created by the stimulus. We will refer to this as H_S, a head-centric value, in order to distinguish it from the retinal shear disparity H_R. In the upper row, the eyes are torsionally aligned ($\tau = 0$) and are fixating a frontoparallel plane. H_S is 0 near the fixation point. Slant can be recovered from equations (1) and (2). In the middle row, the eyes are again torsionally aligned, but the plane is now slanted about a horizontal axis ($S < 0$; $H_S > 0$; $\tau = 0$); again slant can be recovered accurately from equations (1) and (2). In the lower row, the plane is slanted by the same amount as in the middle row, but the eyes are extorted. The shear disparity at the retinas is $H_R = H_S - \tau$. Thus, a particular combination of slant and extortion creates a pattern of horizontal-shear disparity identical to the pattern created by a frontoparallel plane when the eyes are aligned (upper row). If we do not know the torsional state of the eyes,

the slant specified by H_R is ambiguous (Ogle & Ellerbrock, 1946; Howard & Kaneko, 1994).

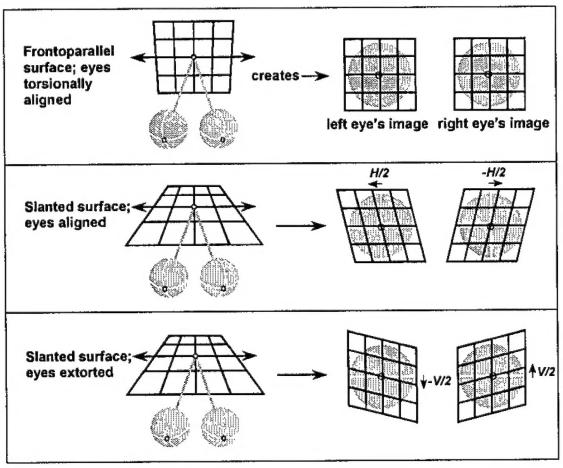

Figure 1.7. Cyclovergence affects the relationship between slant and horizontal-shear disparity. In each of the three panels, the left side depicts the viewing situation and the right side the shear disparities at the retinas. Upper panel: The observer is viewing a frontoparallel plane with the eyes torsionally aligned ($\tau = 0$). The horizontal-shear disparity is 0. (Note that we have not shown the gradients of vertical disparity that would occur with the viewing of objects at non-infinite distances.) Middle panel: The plane is slanted about a horizontal axis (slant < 0) which creates a positive horizontal-shear disparity. Horizontal-shear disparity is the difference between the orientations of the images of a vertical (right eye minus left eye): $- H_R /2 - H_L /2 = - H_R$. Lower panel: The plane is again slanted about a horizontal axis, but the eyes are also extorted ($\tau > 0$) such that the horizontal-shear disparity is 0. If the visual system did not compensate for the horizontal shear created by cyclovergence, slant would be misestimated.

The need to compensate for changes in the eyes' horizontal vergence and cyclovergence is further illustrated in Figure 1.8. Each panel shows the slant estimate obtained from equation (1.3) as a function of distance (which can be estimated from μ). The horizontal-shear disparity observed at the retinas (H_R) is 0, –1, and –2 deg in the upper, middle, and lower panels, respectively. Each panel shows five curves that correspond to the estimate from equation (1.3) for cyclovergences of –4, –2, 0, 2, and 4 deg. The correct surface slant is indicated by the thick curve in each panel ($\tau = 0$). Estimates obtained from equation (1.4) are indicated by the open circles. Clearly, failure to compensate for cyclovergence can have a profound effect on the estimated slant; for example, at a distance of 100 cm, the estimation error is –47.5, –28.6, 0, 28.6, and 47.5 deg for cyclovergences of 4, 2, 0, –2, and –4 deg, respectively. Likewise, failure to compensate for changes in horizontal vergence (correlate of distance) can have a large effect on the slant estimate; for example, when H_R = –2 deg (lower panel) and the eyes are torsionally aligned ($\tau = 0$), the correct slant varies from ~0 deg at very near distances to 47.5 deg at 200 cm. Here we ask whether the visual system compensates for changes in cyclovergence and horizontal vergence and, if it does compensate, the means by which the compensation is accomplished.

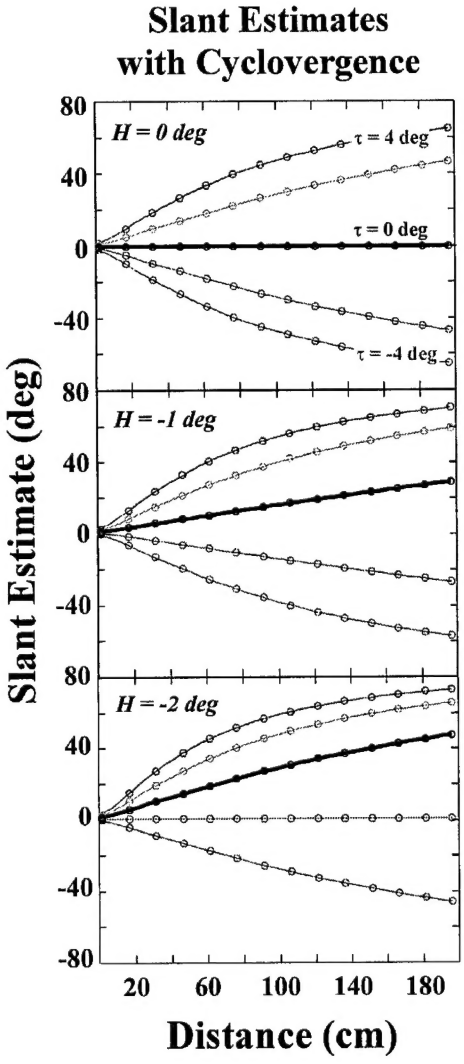

Figure 1.8. Slant estimates as a function of distance, slant, and cyclovergence. Each panel plots the slant estimate as a function of distance for a given horizontal-shear disparity (H_R). The upper, middle, and lower panels show the estimates when H_R = 0, –1, and –2 deg, respectively. The true slant in each panel is indicated by the black curve. The five curves in each panel represent the estimates when the cyclovergence (τ) is –4, –2, 0, 2, and 4 deg. The slant estimates derived from Equation (1) are indicated by the thin colored curves and the estimates derived from Equation (2) by the small circles. Equation (2) provides an excellent approximation to Equation (1). It is important to note the large errors in slant estimation that would occur if there were no compensation for the effects of cyclovergence.

The visual system could in principle compensate for cyclovergence and horizontal vergence by use of extra-retinal signals. In particular,

$$S \approx -\tan^{-1}[\frac{1}{\mu}\tan(H_R + \hat{\tau})] \qquad (1.5)$$

where $\hat{\tau}$ is an extra-retinal, cyclovergence signal and μ is the horizontal vergence and could be measured by an extra-retinal vergence signal. If the extra-retinal, cyclovergence signal is accurate, $\hat{\tau} = \tau$. To our knowledge, there is no evidence that an extra-retinal torsion signal exists (see Nakayama & Balliet, 1977), but the possibility should be entertained because it has been shown that extra-retinal signals of horizontal version and horizontal vergence are used in interpreting horizontal disparity patterns (e.g., Backus, et al., 1999; Rogers & Bradshaw, 1995).

The visual system could also compensate for cyclovergence by use of vertical-shear disparity. Cyclovergence and slant about a horizontal axis produce different effects on the retinal images; specifically, cyclovergence alters the pattern of vertical disparities at the horizontal meridians of the eyes, but horizontal-axis slant changes do not (Rogers, 1992; Howard, Ohmi, & Sun, 1993; Howard & Kaneko, 1994). This is illustrated in the middle and lower panels of Figure 1.7.

Vertical-shear disparity (V_R) can be defined as the angle between the projections of a horizontal line in the two eyes (lower panel, Figure 1.7). Slant about the horizontal axis is given to close approximation by:

$$S \approx -\tan^{-1}[\frac{1}{\mu}\tan(H_R - V_R)]. \qquad (1.6)$$

So the visual system could, in principle, estimate slant even when the eyes are torsionally misaligned by measuring H_R, V_R, and distance. This equation predicts that changes in perceived slant can be induced by altering H_R or V_R, and such an effect has been demonstrated by Ogle and Ellerbrock (1946), Howard and Kaneko (1994), and others.

There is, of course, a variety of monocular slant signals that can be used to estimate slant about a horizontal axis. The most obvious such signal is the texture gradient which can be used to estimate surface slant and tilt (Gibson, 1950; Knill, 1998). The utility of the texture gradient is unaffected by cyclovergence and horizontal vergence, so the visual system would not have to compensate for vergence changes when using this slant signal to estimate local surface orientation. We were able to eliminate the influence of these signals in the work presented here, so we focus only on disparity and extra-retinal signals.

There is clear experimental evidence that the visual system can use both extra-retinal signals and patterns of vertical disparity to compensate for changes in horizontal vergence. Thus, we will focus here on cyclovergence. There are three possible means of compensation.

1. Perhaps compensation does not occur, so cyclovergence changes lead to errors in slant estimation like those shown in Figure 3. We will refer to this as the *no-compensation model.* It is represented quantitatively by equations (1.3) and (1.4).
2. Perhaps compensation occurs via use of an extra-retinal torsion signal. We will refer to this as the *extra-retinal-compensation model.* It is represented quantitatively by equation (1.5).
3. Perhaps compensation occurs via use of vertical-shear disparity. We will refer to this as the *vertical-disparity-compensation model* and it is represented by equation (1.6).

Usually, greater slant is perceived in stereo-defined surfaces when slant is about the horizontal axis as opposed to the vertical axis (Rogers & Graham, 1983; Mitchison & McKee, 1990; Gillam & Ryan, 1992; Buckley & Frisby, 1993). Because the signals involved are so different for slant estimation about the horizontal axis than for estimation about the vertical axis, there is a variety of possible explanations for this so-called slant anisotropy. Comparing the results from the horizontal axis experiments with our previous work (e.g., Backus et al, 1999) will help delineate the critical differences.

In the experiments we varied cyclovergence and vertical-shear disparity independently to determine whether the two estimation methods exist and, if so, how their outputs are combined. The experimental procedure is depicted in Figure 1.9. We induced cyclovergence with a conditioning stimulus composed of horizontal lines; the lines were rotated in opposite directions in the two eyes. We measured cyclovergence response using a nonius technique. The nonius figure (upper right panel) was flashed and the observer judged whether the lines were subjectively parallel. We validated the nonius technique by using 3-D search coils in van den Berg's lab in Rotterdam. Observers performed the nonius task while eye position was measured. Nonius and objective measures agreed closely (Hooge et al, 2000).

In Experiment 2 (we don't describe Experiment 1 here), the stimulus used to measure perceived slant was a large random-dot plane; the dots were back-projected to render nonstereo slant signals uninformative. Different amounts of vertical-shear disparity were added to the stimulus. The plane was

flashed and the observer adjusted horizontal-shear disparity until the plane appeared gaze normal (lower right panel). The procedure cycled between the conditioning stimulus (2 sec), nonius figure (100 msec), conditioning stimulus (2 sec), test stimulus (100 msec), and so forth until the observer was satisfied with both settings. By using this procedure, we knew the eyes' cyclovergence.

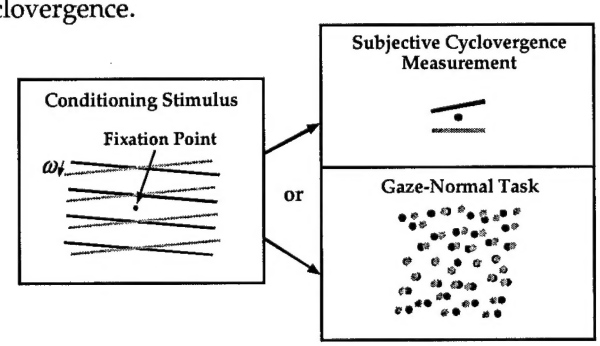

Figure 1.9. Experimental procedure. Black lines represent left eye's image and gray lines right eye's image. Conditioning stimulus (left) is presented to induce cyclovergence. Nonius technique (upper right) is used to measure cyclovergence; observers adjust orientation of upper line until subjectively parallel to lower. Gaze-normal task (lower right) is used to measure slant percepts. Observers adjust *HSh* until random-dot plane appears gaze normal.

Predictions for the gaze-normal task are represented by the diagonal lines in Figure 1.10. Cyclovergence response is plotted on the abscissa and horizontal-shear disparity (at the retinae) on the ordinate. If no compensation occurred for changes in cyclovergence, gaze-normal settings would be predicted by Equation (1.4); the data would lie on the horizontal line. If complete compensation occurred based on vertical-shear disparity (Equation 1.6), the data would lie on the five diagonal lines (one for each amount of added vertical disparity). If complete compensation occurred based on eye-position signals (Equation 1.5), data would lie on the central diagonal line.

Data from one of the three observers are shown in the right panel of Figure 8. The data are clearly most consistent with compensation by vertical-shear disparity (Eqn 1.6). Data from the other two observers were quite similar.

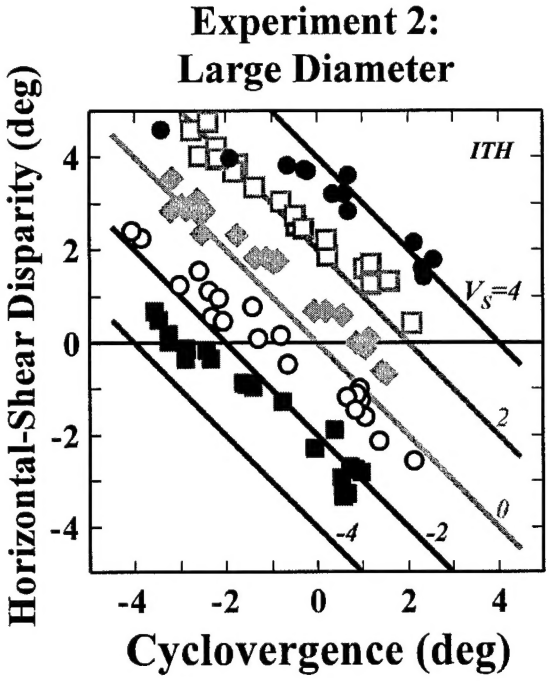

Figure 1.10. Experiment 2 results for observer ITH. The horizontal-shear disparity that appeared gaze normal is plotted as a function of cyclovergence. Horizontal shear is in retinal coordinates. Stimulus diameter was 35 deg. Vertical-shear disparity (in head-centric coordinates) was –4, –2, 0, 2, or 4 deg; each is represented by a different data symbol. Vertical shear at the retinas was the sum of the vertical shear added to the stimulus plus the effect of cyclovergence. If no compensation for cyclovergence occurred, the data would lie on the horizontal line. If veridical compensation based on use of vertical-shear disparity occurred (Equation 1.6), the data would lie on the diagonal lines. If veridical compensation based on use of an extra-retinal, cyclovergence signal occurred (Equation 1.5), the data would lie on the central diagonal line. Each data point represents one setting.

Experiments 3 and 4 were designed to determine whether there is any influence of extra-retinal, torsion signals. In Experiment 3, we reduced the diameter of the random-dot plane to 5 deg; this made vertical-shear disparity difficult to measure. In Experiment 4, the stimulus was a single smooth vertical line; this makes vertical-shear disparity impossible to measure because there are no vertically separated features. In both cases, we found a complete failure to compensate for the eyes' cyclovergence. In other words, when we induced cyclovergence changes, the observer saw different slants in the stimulus. It appears then that compensation for cyclovergence is mediated only by use of vertical disparities. We found no evidence for use of an extra-retinal signal.

During the past year, we completed two more manuscripts on visual space perception.

One was an investigation into the perception of slant with real-world objects. In collaboration with Fiona James, Keith Humphrey and Tutis Vilis of the University of Western Ontario, we examined how people take eye position into account when asked to judge the slant of a surface in world coordinates. To judge slant relative to the world, the nervous system must measure surface slant relative to the line of sight (oculocentric slant), eye position relative to the head, and head position relative to the world coordinates. We showed two things: 1) people are quite good at judging object slant in world coordinates and 2) their errors are the outcome of errors in all three measurements. This work is currently in press in *Vision Research* (James, Whitehead, Humphrey, Banks, & Vilis, 2001).

The other manuscript reports an investigation into the means by which we estimate the horizontal eccentricity of an object relative to the head. There are two quite different methods by which the nervous system could estimate the head-centric eccentricity of an object.

The first method is the obvious one. Measured from the cyclopean eye, the horizontal eccentricity or azimuth of an object point is given by the average of α_L and α_R; this quantity is called the horizontal version of the eyes, γ. Thus, an observer can in principle estimate a fixated object's azimuth, a, from γ. If the observer is not fixating the object, the azimuth is the sum of the retinal image eccentricity (r; which is the average of the retinal eccentricities in the two eyes) and the version: $a = r + \gamma$. Azimuth is, therefore, given by:

$$\hat{a} = \hat{r} + \hat{\gamma} \qquad (1.7)$$

where the hats signify measurements of the relevant quantities.

The second method is less obvious and does not require the use of eye-position signals. If an object is to the left of the head's median plane, it is guaranteed to be taller in the left eye than in the right eye. If it is to the right of the median plane, it will be taller in the right eye. In this manuscript we showed that one could in principle estimate head-centric eccentricity in the following way.

$$a \approx \tan^{-1}\left(\frac{\ln VSR}{\mu}\right) \qquad (1.8)$$

where VSR is the vertical size ratio (a measure of vertical disparity) and μ is the eyes' vergence (which can be obtained from retinal information alone).

We asked which method the visual system uses in estimating the horizontal eccentricity of an object. On each trial, a large, random-dot surface was presented at a chosen horizontal eccentricity. The observers had to turn the eyes by different amounts (different horizontal versions) to fixate the center of the surface. The eye-position-specified azimuth of the stimulus was how far the eyes had to turn left or right; the vertical-disparity-specified azimuth was the pattern of vertical disparities presented to the eyes (taller in the left eye when the disparity-specified azimuth was to the left). Observers pointed in the perceived direction of the center of the stimulus with an invisible pointer held by the two hands. The data from one observer are presented in Figure 1.11 (the other observers yielded very similar data). The azimuth of the pointing response is plotted as a function of the eye-position-specified azimuth of the stimulus. The different symbols represent data for different disparity-specified azimuths. Clearly, the eye-position-specified azimuth was the sole determinant of perceived direction. Thus, the method suggested by Eqn. 1.7 seems to be employed by the nervous system.

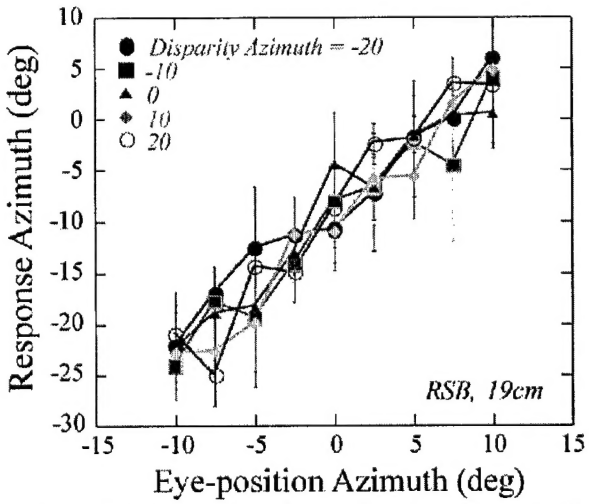

Figure 1.11. Response azimuth as a function of eye-position-specified azimuth for a viewing distance of 19 cm. The azimuths of the observer's responses are plotted as a function of the eye-position-specified azimuth. Different disparity-specified azimuths are represented by different symbols. The error bars indicate +/--1 standard deviation.

The manuscript describing this work is in press at *Vision Research* (Banks, Backus, & Banks, 2001).

2. Heading Perception

We have also continued our research on the perception of self-motion. In the previous review

period, five publications appeared from this project: Crowell et al (1998), Ehrlich et al (1998), Freeman and Banks (1998), Freeman (1999), and Freeman et al (2000). In this last grant period, we have completed the theoretical analysis and experiments on another project that was reported at ARVO (Sibigtroth & Banks, 2000). We also completed construction of our 3-axis rotating chair in which we are conducting visual-vestibular research that is relevant to spatial disorientation in aviation. We are approximately half-way through the first set of experiments on visual-vestibular interactions. We presented preliminary data at VSS (Sibigtroth & Banks, 2001).

As in the previous section, we will first review the background material for this research project before moving onto the particular experiments and analyses that were completed. Much of this background section also appeared in the previous progress report, so if you read it, you may want to skip ahead to page 11.

As a person moves through the environment, images move across the retina, the eyes move relative to the head, the head turns relative to the body, and the body translates and rotates through space. Despite this complex of various motions, the nervous system produces a coherent percept of the person's motion relative to environmental landmarks. From this percept, the human observer is able to move toward targets, avoid obstacles, and guide complicated perceptual-motor behavior. We have been examining how the nervous system accomplishes this. Our work has examined the analysis of visual signals, eye-velocity signals, head-velocity signals, and more.

We continued our work on the use of various signals to estimate the direction of self-motion. The problem we examined in the *rotation problem*, so we begin with a description of that problem, followed by a brief literature review, and then by a description of our work during the grant period.

As we move through the environment, the retinal image of that environment changes in predictable ways. For example, if we move in a straight line our self-motion produces a radial pattern of motion in the retinal image, like that in Figure 2.1A. The center or focus of the radial expansion (marked by a '+' in Figure 15) corresponds to our direction of motion (Gibson, et al, 1955). Re-creating this pattern of retinal-image motion by viewing a film or computer display depicting our forward motion can cause a compelling sensation that we are in fact moving forward (Howard, 1982), and under a variety of conditions we can accurately estimate where we are going in the simulated scene (Warren et al, 1988; Royden et al, 1992).

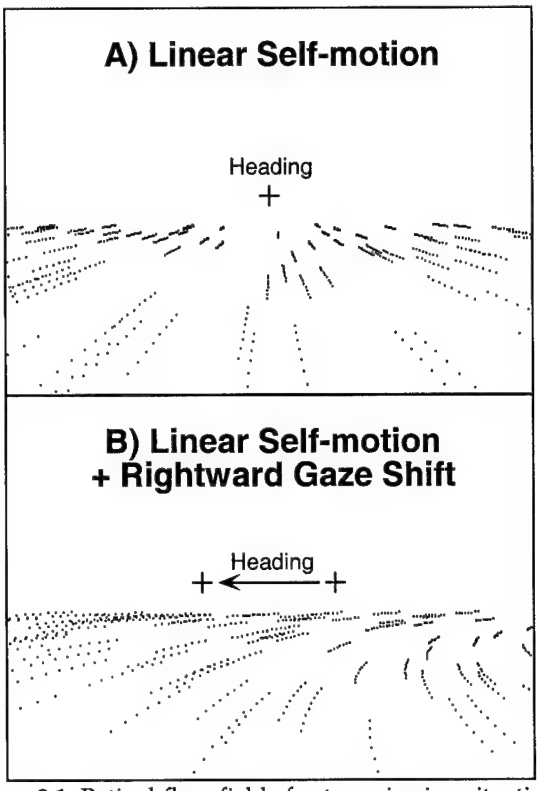

Figure 2.1. Retinal flow fields for two viewing situations. A) Forward translation without a gaze rotation. Observer is fixating in constant direction and heading toward the cross. B) Forward translation while making a gaze rotation. Observer is making a rightward eye movement.

When we smoothly shift gaze direction by turning the eye or head (e.g. to look at a moving object or a stationary object to the side) while still moving in a straight line, the pattern of retinal-image motion is more complex (Figure 2.1B). We can re-create this type of retinal motion pattern by having observers hold the eyes still while viewing a display that simulates both their forward motion and an eye movement. In this case, observers report that they are moving along a curved trajectory (as though turning a car while looking forward through the windshield) rather than along the depicted linear path. When they are asked to adjust the position of a marker in front of them until it appears to sit upon their future path, their responses are strongly biased in the direction of the perceived path curvature (Royden et al, 1992, 1994; Banks et al, 1996; van den Berg, 1996). On the other hand, self-motion judgments are quite accurate when the identical pattern of retinal image motion is created by having observers view a display like that in Figure 2.1A while turning the eye to pursue a target that moves across it (Royden et al, 1992, 1994; Banks et al, 1996; van den Berg, 1996). Observers typically report that they appear to be moving on a straight rather than a curved path (Royden, 1994). In this case, the observer's visual

system has extra-retinal information about the eye movement, probably consisting mainly of an efference copy of the motor command to turn the eye (Howard, 1982). The visual system uses this information to compensate for the effects of the eye movement on the retinal motion pattern; previous research using self-motion judgments indicates that this compensation is nearly complete.

We completed an investigation of how perspective transformations affect humans' ability to estimate self-motion. The first set of experiments was presented at ARVO (Sibigtroth & Banks, 2000). The optic flow field created by self-motion through a rigid environment is an important cue to direction of self motion, but it is not the only visual cue. Consider, for example, the case when you walk by a rectilinear frame (depicted in Figure 2.2). If you pass to the left side of the frame, you will see the left side grow more in visual angle than the right side. If you pass to the right, the opposite will occur. Can the visual system take advantage of this perspective information (assuming that the frame is indeed rectilinear) to estimate the heading? Jeremy Beer at Brooks AFB had a similar insight a few years ago and showed the people are sensitive to this information. During the grant period, we worked through the mathematics and showed how this perspective transformation information could be used to determine the direction of self-motion. We then conducted experiments (presented at ARVO) that showed that human observers do indeed use this information to estimate heading. This summer we are completing some control experiments before writing the work up for publication.

During the grant period, we completed construction of our three-axis rotating chair. We began to investigate how stimulation of the otoliths (the parts of the vestibular apparatus that signal linear acceleration) affects the perception of heading. Such investigations are clearly relevant to understanding visual-vestibular illusions that occur in aviation such as the pitch-up (somatogravic) illusion and the bank illusion (which can lead to the death spiral).

We presented subjects optic flow displays simulating forward translation and a gaze rotation (see Figure 2.1B). Normally, observers say they perceive curvilinear self-motion with such displays. We found, however, if we rolled observers to simulate correct or incorrect centrifugal force, we could bias their percepts of self-motion path.

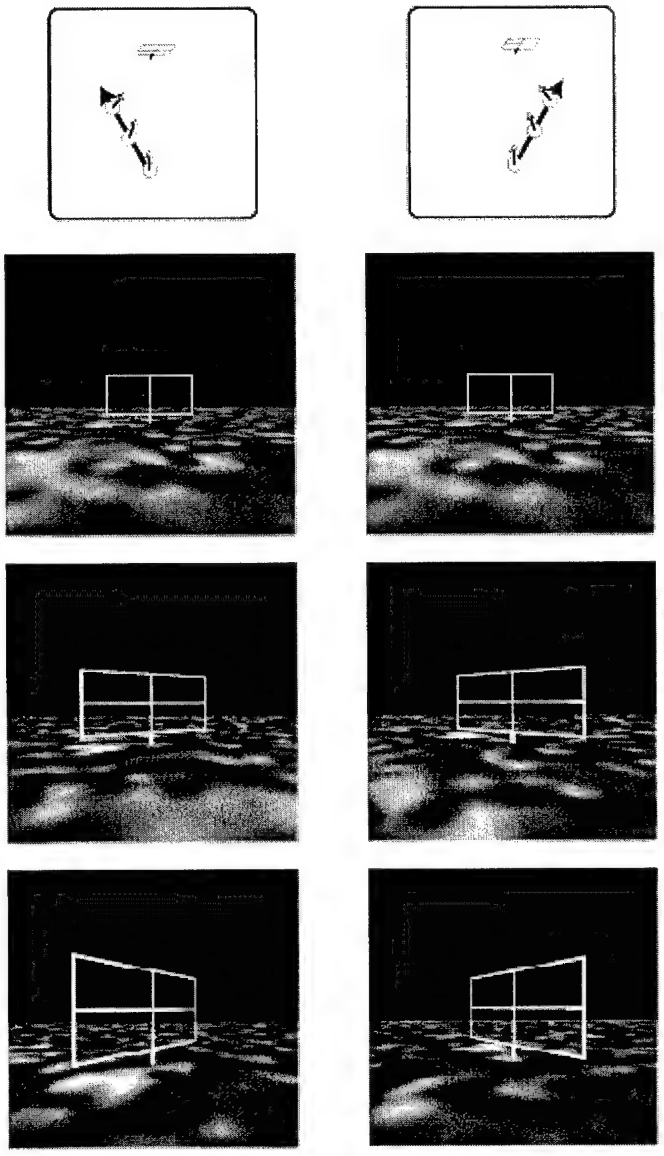

Figure 2.2. Upper panels: Plan views of two different self-motion paths. The paths are represented by the successive positions of the eyes. The gaze directions are represented by the arrows from the eyes. The rectilinear frame is shown in the upper part of both panels. Other panels show the view sequences associated with those two paths. Notice the change in the projected shape of the rectilinear frame.

We also investigated the role of otolith signals in the estimation of self-motion paths. As we explained above, an observer on a linear path making a smooth horizontal eye movement to the right creates optic flow that is very similar to an observer on a curvilinear path with the curvature to the right (Royden, 1994). As we have shown earlier, observers tend to see curvilinear paths when optic flow consistent with a linear path is presented unless the gaze rotation is accompanied by either an extra-retinal, eye-velocity signal or an extra-retinal, head-velocity signal (e.g., neck proprioceptors and semi-circular canals). Notice that if an observer is

on a curvilinear path (left side of Figure 2.3), the centripedal acceleration to the right creates leftward centrifugal force (labeled "a" in the middle of Figure 2.3). An observer on a linear path making a gaze rotation to the right will not experience this centrifugal force. If the otoliths sensed the centrifugal force, they could aid in the disambiguation of linear vs curvilinear self-motion. We tested this hypothesis during the grant review period.

We completed the software for our 3-axis rotating chair so we can rotate the observer about the pitch, roll, and yaw axes while he/she views motion sequences on a projection screen that moves with the chair. To determine whether the otolith signals are used in the estimation of self-motion paths we presented optic flow sequences consistent with linear paths (with simulated gaze rotation) or curvilinear paths while the observer either sat upright or was rolled to simulate centrifugal force (right side of Figure 2.3). We asked the observers to report on their future perceived position relative to a landmark that appear in the visual scene at the end of the motion sequence.

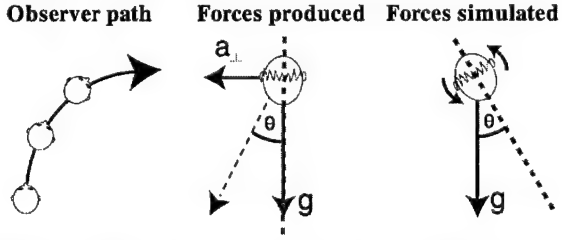

Figure 2.3. Scenarios involved in curved self-motion paths. Left: circular path curving to the right. Observer's gaze direction maintains constant relationship to the path, so it rotates over time. Middle: forces created on circular path. The gravitational force is represented by *g* and the outward centrifugal force by *a*. The net force is the vector sum, g + a, which is a force at angle Θ relative to the head. Right: we can simulate this situation by rolling the observer's head through angle Θ.

The results are shown in Figure 2.4. The panel on the left shows data when the motion sequence simulated linear paths and the one on the right shows data when the sequence simulated curvilinear paths. The graphs plot the error in the perceived path as a function of the gaze rotation rate. If performance were veridical, the data would fall on the horizontal dashed line.

When a linear path was presented (left panel), observers reported more curved paths when they were rolled ("otolith inconsistent"; circular data symbols) than when they were upright ("otolith consistent"; square symbols). When a curvilinear path was presented (right panel), observers again reported more curved paths when they were rolled ("otolith consistent"; circles) than when they were not ("otolith inconsistent"; squares). These results show that the otolith signal does indeed affect heading judgments.

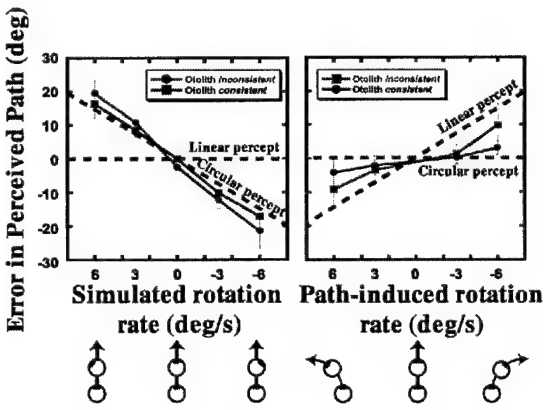

Figure 2.4. Results from visual-otolith experiment. Both panels plot the error in the perceived path (in deg) as a function of the gaze rotation rate. Left panel: the optic flow sequence simulated a linear path with gaze rotation. If responses were veridical, the data would lie on the horizontal dashed line. When the observer was rolled (otolith inconsistent; circles), he/she reported more path curvature than when he/she was not rolled (otolith consistent; squares). Right panel: the optic flow sequence simulated a circular path with gaze rotation due to the path curvature. If responses were veridical, the data would lie on the horizontal dashed line. When the observer was rolled (otolith consistent; circles), he/she reported more path curvature than when he/she was not rolled (otolith inconsistent; squares).

3. Visual-Haptic Integration

During the grant period, we purchased equipment and constructed an apparatus for studying visual-haptic integration. The major equipment purchase was for two PHANToM force-feedback devices that allow one to simulate haptic stimuli; these monies were provided by AFOSR in an equipment supplement grant. We were also given an OnyxII graphics workstation from Silicon Graphics to serve as host for the PHANToMs.

The experimental setup is schematized in Figure 3.1. The visual display is viewed in a mirror placed above the hand. The index finger and thumb of the right hand are placed in separate haptic feedback devices (depicted beneath the mirror). The PHANToMs feedback devices provided force to the finger and thumb and thereby simulated a virtual object or surface.

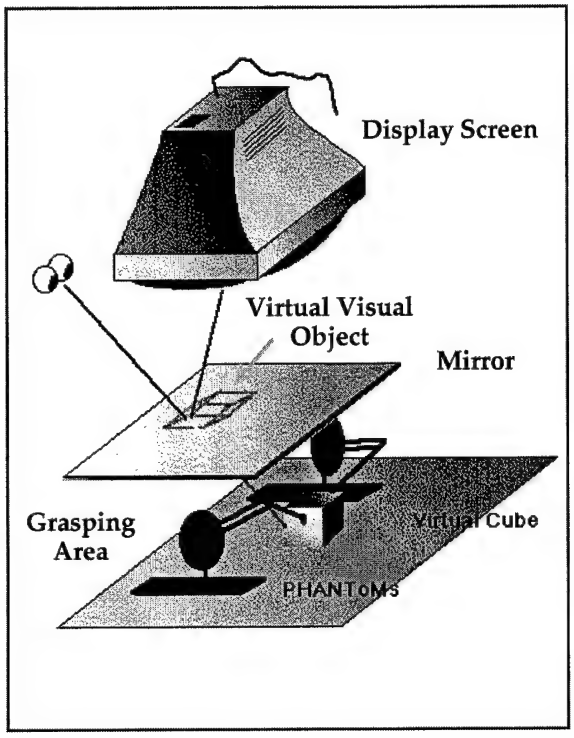

Figure 3.1. The experimental setup for the visual-haptic integration experiments. The visual stimulus is presented in the display screen above and viewed in the mirror placed above the hand. The index finger and thumb of the right hand are placed in PHANToMs haptic feedback devices. The observer touches and grasps virtual objects in the workspace. Haptic feedback creates the sensation of touching a real object or surface.

During the grant period before this one, we completed an experiment on the use of haptic information to set the weights given to different visual cues. This work appeared in *Nature Neuroscience* (Ernst, Banks, & Buelthoff, 2000). It was conducted in Germany. During this last grant period, we completed an experiment on visual-haptic integration and the manuscript describing this work was recently accepted in *Nature* (Ernst & Banks, 2001). We describe this experiment here.

When a person looks at an object while exploring it with the hand, vision and touch both provide useful information for estimating the object's properties. Frequently, vision dominates the integrated, visual-haptic percept—such as when judging size, shape, or position (Rock & Victor, 1964)—but in some circumstances, the percept is clearly affected by haptics (Power, 1980). If the human observer uses vision and haptics to estimate an environmental property (e.g., an object's size), it would be sensible to do it in a way that minimizes error in the final estimate. This general principle—minimizing variance in the final estimate—can be realized by using maximum-likelihood estimation (MLE; Landy et al, 1995; Gharamani et al, 1997) to combine the inputs.

A sensory system's estimate of an environmental property can be represented by:

$$\hat{S}_i = f_i(S) \qquad (3.1)$$

where S is the physical property being estimated and f the operation by which the nervous system does the estimation. The subscripts refer to the modality (i could also refer to different cues within a modality). Each sensor's estimate, $\hat{S}_i$, is corrupted by noise. If the noises are independent and Gaussian with variance σ_i^2 and the Bayesian prior is uniform, MLE of the environmental property is given by:

$$\hat{S} = \sum_i w_i \hat{S}_i \quad \text{with:} \qquad w_i = \frac{1/\sigma_i^2}{\sum_j 1/\sigma_j^2} \qquad (3.2).$$

Thus, the MLE rule states that the optimal means of estimation is to add the sensor estimates weighted by their normalized reciprocal variance (Landy et al, 1995). If the MLE rule is used to combine visual and haptic estimates, $\hat{S}_V$ and $\hat{S}_H$, the variance of the final (visual-haptic) estimate, $\hat{S}$, is:

$$\sigma_{VH}^2 = \frac{\sigma_V^2 \sigma_H^2}{\sigma_V^2 + \sigma_H^2} \qquad (3.3).$$

Thus, the final estimate has lower variance than either the visual or haptic estimator.

Here we examine visual-haptic integration quantitatively to determine whether human performance is optimal. Observers looked at and/or felt a raised ridge and judged its height (vertical extent). To work out the predictions of the MLE rule, we first determined the variances of the visual and haptic height estimates (within-modality) by conducting discrimination experiments. In the haptic-alone experiment, observers indicated which of two sequentially presented ridges was taller from haptic information alone; in the visual-alone experiment, they did the same from vision alone. There were four conditions in the visual experiment differing in the amount of noise in the stimulus. By adding noise we made the visually specified height less reliable.

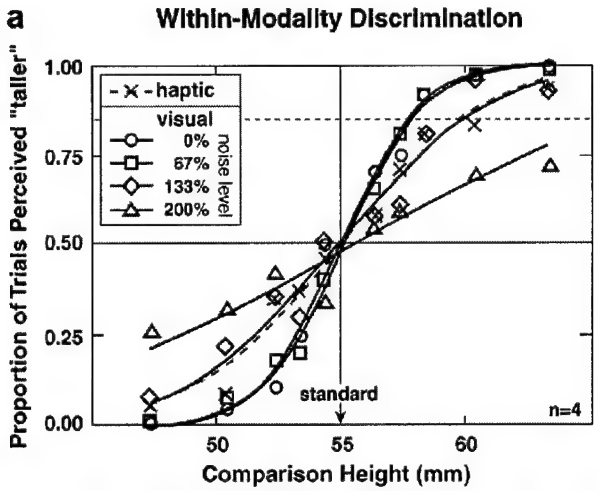

Figure 3.2A. Within-modality discrimination data. The proportion of trials in which the comparison stimulus was perceived as taller than the standard stimulus is plotted as a function of the comparison's height. Data have been averaged across the four observers. The standard's height was always 55mm. The haptic discrimination data are represented by the x's and the best-fitting cumulative Gaussian by the dashed curve. The visual discrimination data are represented by the four open symbols and solid curves. Each corresponds to a different level of visual noise.

Fig. 3.2a shows the visual-alone and haptic-alone discrimination data. The proportion of trials in which the observer indicated that the comparison stimulus (variable height) appeared taller than the standard stimulus (fixed height of 55mm) is plotted as a function of the comparison's height. The dashed line and symbols represent the haptic discrimination data and the solid curves with open symbols represent the visual data for the four levels of noise. These psychometric functions were well fit by cumulative Gaussians. Discrimination threshold is defined as the difference between the PSE and height of the comparison stimulus when it is judged taller than the standard 84% of the time. The 84% points correspond to $\sqrt{2}$ times the standard deviation of the underlying estimator. The haptic discrimination threshold was approximately 0.085 times the average ridge height (which was 55mm). As the noise increased from 0% to 200%, the visual discrimination thresholds increased from 0.04 to 0.2 times the average height. Thus, when the visual noise was 0%, the visual discrimination threshold was roughly half the haptic threshold; when the visual noise was 200%, the visual threshold was more than double the haptic threshold.

In the visual-haptic experiment, observers simultaneously looked at and felt two raised ridges that were presented sequentially. In one presentation, the visually and haptically specified heights were equal (*comparison stimulus*), in the other presentation, they differed (*standard stimulus*). The difference in the specified heights was Δ=±6, ±3, or 0mm (average of S_H and S_V was 55mm). For each Δ in the standard (randomly presented), the height of the comparison stimulus was varied (47-63mm) randomly from trial to trial. On each trial, the observer indicated which stimulus seemed taller.

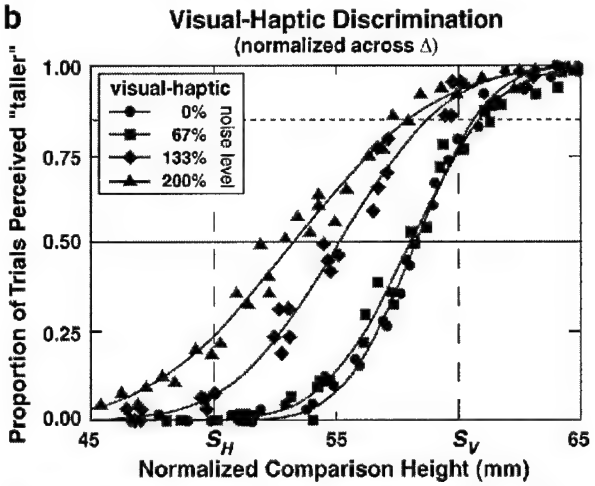

Figure 3.2.B. Visual-haptic discrimination data. The proportion of trials in which the comparison stimulus was perceived as taller than the standard stimulus is plotted as a function of the comparison's height. The standard's average height was always 55mm, but the difference between the visually and haptically specified heights varied from –6 to 6mm. To plot the data on one set of coordinates, we shifted the psychometric functions laterally by $w_v\Delta/2$. The four sets of symbols correspond to different levels of visual noise.

Fig. 3.2b shows the proportion of trials in which the comparison stimulus was chosen as taller as a function of the comparison's height. From those psychometric functions, we obtained the point of subjective equality (PSE)—the comparison height appearing equal to the standard height—and the just-discriminable change in height (threshold).

Using the within-modality data, we can now predict what an observer using MLE would do when presented visual and haptic information simultaneously and then compare those predictions to the performance in the visual-haptic experiment.

We first describe the analysis of the PSE data and predictions for the weights. From Eqn. (3.2) and the relationship between threshold and estimator variance:

$$\frac{w_V}{w_H} = \frac{\sigma_H^2}{\sigma_V^2} = \frac{T_H^2}{T_V^2}$$

where T_H and T_V are the haptic and visual thresholds (84% points in Fig. 3.2a). Incorporating the

normalization assumption ($w_V + w_H = 1$), the predicted weights for optimal integration are:

$$w_V = \frac{T_H^2}{T_V^2 + T_H^2} \quad \text{and} \quad w_H = \frac{T_V^2}{T_V^2 + T_H^2} \qquad (3.4).$$

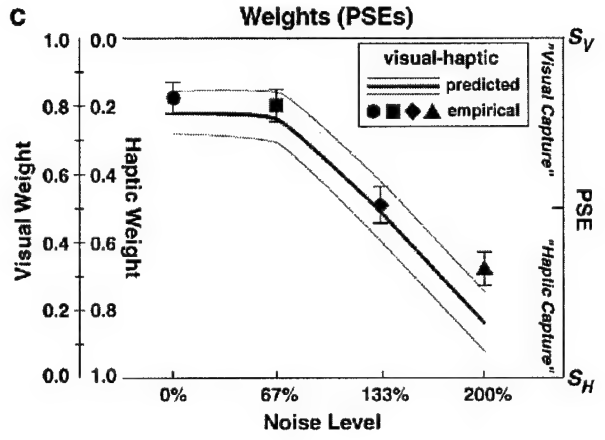

Figure 3.2.C. Observed and predicted weights and PSEs in visual-haptic judgments. The abscissa is the amount of visual noise. The left ordinate is the visual weight. The right ordinate is the PSEs in relation to SV and SH. The purple symbols represent the observed visual weights based on the observers' PSEs in the visual-haptic experiment (Fig 3b; Eqn 3.5). The shaded area represents the weights expected from the within-modality discrimination data (Fig 3a; Eqn 3.4).

The predicted visual weights are represented by the curve and shaded surround in Fig. 3.2c. The predicted weights vary significantly with the amount of visual noise in the stimulus: the visual weights are higher when the noise level is low and lower when the noise level is high. Assuming that the visual and haptic estimators are on average unbiased ($\hat{S}_V = S_V$ and $\hat{S}_H = S_H$), the weights can be derived experimentally:

$$w_v = (PSE - S_H)/(S_V - S_H) \qquad (3.5)$$

where *PSE* is the height of the comparison stimulus that matched the apparent height of the standard. The visually and haptically specified heights in the standard—S_V and S_H—are indicated on the right ordinate. Fig. 3.2c shows that as the noise level was increased, the visual weight decreased, and the PSE shifted from S_V toward S_H. Because the noise level varied randomly from trial to trial, the weights must have been set within the 1-sec stimulus presentation. In the discussion we suggest a mechanism for such dynamic weight adjustment. To summarize, the predicted and observed PSEs are quite similar suggesting that humans do combine visual and haptic information in a fashion similar to MLE integration.

We now turn to the analysis of the visual-haptic discrimination thresholds. According to the MLE rule, the combined estimates should have lower variance, and therefore lower discrimination thresholds, than either the visual or haptic estimate alone (Eqn. 3.3). To derive predictions for the visual-haptic discrimination thresholds, we rewrite Eqn. 3:

$$T_{VH}^2 = \frac{T_V^2 T_H^2}{T_V^2 + T_H^2} \quad \Leftrightarrow \quad \frac{1}{T_{VH}^2} = \frac{1}{T_V^2} + \frac{1}{T_H^2} \qquad (3.6)$$

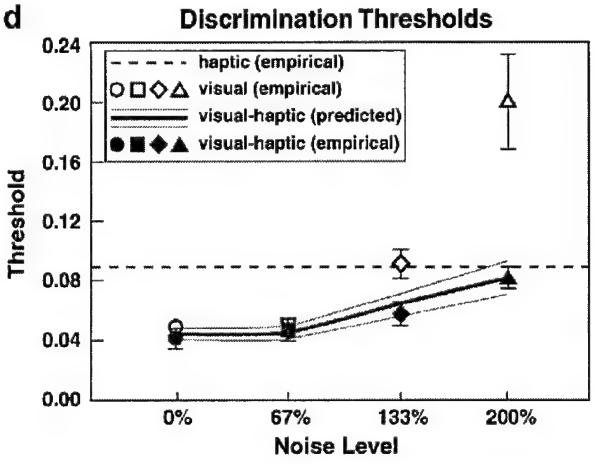

Figure 3.2.D. Within-modality and visual-haptic discrimination thresholds. The just-noticeable difference in height is plotted as a function of the visual noise. The threshold values are taken from the psychometric functions of A and B above; they correspond with the difference between the PSE and the comparison height that was chosen on 84% of the trials as taller than the standard height. The dashed horizontal line represents the haptic-alone threshold. The open symbols represent the vision-alone thresholds. The filled symbols represents the visual-haptic thresholds and the gray shaded area the predicted visual-haptic thresholds (Eqn 3.6).

Fig. 3.2d shows the predicted and observed thresholds. The unfilled symbols represent the visual-alone thresholds and the dashed line represents the haptic-alone threshold. The shaded area represents the predicted visual-haptic thresholds; they are always lower than the visual-alone and haptic-alone thresholds at the corresponding noise level. The filled purple points represent the observed visual-haptic discrimination thresholds; as noise level increased, the just-noticeable difference in height became greater. Most importantly, the predicted and observed visual-haptic discrimination thresholds are quite similar. As with the PSE data, this suggests that human observers

combine visual and haptic information in a fashion similar to MLE integration.

In summary, we found that height judgments were remarkably similar to those predicted by the MLE integrator. Thus, the nervous system seems to combine conflicting visual and haptic information in a fashion similar to the MLE rule: visual and haptic estimates are weighted according to their reciprocal variances (Eqn. 3.2). Naturally, it is important to determine whether this rule characterizes the estimation of other stimulus properties such as shape, depth, localization, roughness, and compliance.

The relative contributions of vision and haptics to perceiving such object properties have previously been studied. For example, Rock and Victor (1964) had subjects grasp a square while looking at it through a distorting lens that made it appear rectangular. The shape of the unified percept was determined almost completely by vision, so the phenomenon has been called "visual capture". Numerous studies have replicated visual capture in shape and size perception, depth perception, and localization. However, visual capture does not occur in the perception of surface roughness; rather perceived roughness is affected nearly equally by haptics and vision. Does a dynamic cue-combination rule, like the one described here, determine the degree to which vision or haptics dominates? The statistically optimal means of combining visual and haptic information—the MLE rule—predicts that "visual capture" should occur whenever the visual estimate of a property has much less variance than the haptic estimate. "Haptic capture" should be observed when the reverse occurs. We observed behavior like visual capture when the visual stimulus was noise-free and behavior similar to haptic capture when the visual stimulus was quite noisy (Fig. 3.2c).

4. Software Development

We have spent a great deal of effort over the previous grant periods developing software for psychophysical experimentation. We briefly describe the developments that continued during the grant period. These include development of specialized computer graphics programs, optimized rendering engines and tools needed to generate displays with specific spatial and temporal properties. Stereo 3D, texture mapping, high frame rate animation and real-time digital image manipulations. We have also developed a suite of external device control routines, sensor and actuator interfaces, drivers, control algorithms, feedback loop systems (human motor through computer sensory channels) and low-level video synchronization tools necessary for doing real-time psychophysics experiments. Almost all the tools we are developing are in form of MATLAB shared libraries, external C or assembly programs interfaced to and called from MATLAB. This scheme allows us to tap into powerful high-level programming and analysis features of MATLAB while we implement experiments that require our low-level tools for doing real-time operations. All of our software tools are made available to the public through the Bankslab web page (http://john.berkeley.edu/software.html). They are currently used by many labs around the world.

BitmapTools

BitmapTools is an external MATLAB plugin for generating high-frame rate animations (highest refresh rate possible on the graphics card/monitor). It allows for design and display of both static bitmaps and bitmap movies on Macintosh and Windows NT platforms. BitmapTools is designed around one important premise, to maximize the blitting (RAM to Video Memory transfer) rate. On the Macintosh, BitmapTools takes advantage of PowerPC processor's pipelining architecture through assembly level tweakings. On the PC (NT), high-bandwidth blitting is achieved through hardware-accelerated calls (DirectDraw). Almost all modern graphics cards contain the necessary hardware for BitmapTools. The issue with movie players in general is the unreliable animation frame rate. In BitmapTools, real-time frame rate is guaranteed. Under normal operations (on NT, with no major background processes), a 1024x768 movie can play at 120 hz without missing frames. If a frame is missed for some reason, exact location of the frame(s) in the sequence is reported.

OpenGLTools

OpenGLTools is a MATLAB external shared library (compiled mex file) that incorporates interactive 2D/3D graphics functionality into MATLAB. The main objective is to bridge MATLAB's high-level programming environment with the low-level OpenGL graphics engine. This is useful because MATLAB's data types and syntax are most natural for creation of basic 3D constructs, as well as hierarchical development and manipulation of the more complex graphics objects. OpenGLTools is augmented by a rich collection of operators and functions (toolboxes) embedded in MATLAB. It is designed as a research tool for vision scientists to create interactive visual stimuli with precise control over spatial, luminance and temporal properties. Some of the advanced features include stereo (anaglyph and LCD shutter glasses), texture mapping, lighting, buffer manipulations, image processing filters, and re-programmable interactive

mouse bindings. OpenGLTools is available on MacOS, Windows, and Unix (IRIX), although Windows (NT) is the best supported platform.

FlightTools

FlightTools is a flight simulation construction plugin for MATLAB. Like OpenGLTools, it takes advantage of hardware-accelerated OpenGLTools calls. The user can define scene elements in form of MATLAB matrices and lists and specify a flight path and camera gaze lists. Real-time animation of flight allows interactive control of flight parameters such as pitch, yaw and roll control as well as other parameters used in construction of specific simulation functions.

5. Publications during Grant Period

Referred Journals

1. Backus, B.T. & Banks, M.S. (1999). Estimator reliability and distance scaling in stereoscopic slant perception. *Perception*, **28**, 217–242.
2. Backus, B.T., Banks, M.S., van Ee, R., & Crowell, J.A. (1999). Horizontal and vertical disparity, eye position and stereoscopic slant perception. *Vision Research*, **39**, 1143-1170.
3. Banks, M.S. & Backus, B.T. (1998). Extra-retinal and perspective cues cause the small range of the induced effect. *Vision Research*, **38**, 187–194.
4. Banks, M.S., Hooge, I.T.C., & Backus, B.T. (2001). Perceiving slant about a horizontal axis from stereopsis. *Journal of Vision*, **1**, 55-79.
5. Banks, M.S., Backus, B.T., & Banks, R.S. (2001). Is vertical disparity used to estimate azimuth? *Vision Research*, in press.
6. Crowell, J.A., Banks, M.S., Shenoy, K.V., & Andersen, R.A. (1998). Visual self-motion perception during head turns. *Nature Neuroscience*, **1**, 732-737.
7. Domini, F., Adams, W.J., & Banks, M.S. (2001). 3D aftereffects are due to shape and not disparity adaptation. *Vision Research*, **41**, 2733-2739.
8. Ehrlich, S.M., Beck, D., Backus, B.T., Crowell, J.A., & Banks, M.S. (1998) Depth information and perceived self-motion during simulated gaze rotations. *Vision Research*, **38**, 3129-3145.
9. Ernst, M.0., Banks, M.S., & Bülthoff, H.H. (2000). Touch can change visual slant perception. *Nature Neuroscience*, **3**, 69-73.
10. Ernst, M.O. & Banks, M.S. (2001). Humans integrate visual and haptic information in a statistically optimal fashion. *Nature*, in press.
11. Freeman, T.C.A. (1999). Path perception and Filehne illusion compared: model and data. *Vision Research*, **39**, 2659-2667.
12. Freeman, T.C.A. & Banks, M.S. (1998). Perceived head-centric speed is affected by both extra-retinal and retinal errors. *Vision Research*, **38**, 941-945.
13. Freeman, T.C.A. Crowell, J.A. & Banks, M.S. (2000). Extra-retinal and retinal amplitude and phase errors during Filehne illusion and path perception. *Perception & Psychophysics*, **62**, 900-909.
14. van Ee, R., Banks, M.S., & Backus, B.T. (1999). An analysis of binocular slant contrast. *Perception*, **28**, 1121-1145.
15. van Ee, R., Banks, M.S., & Backus, B.T. (1999). Perceived visual direction near an occluder. *Vision Research*, **39**, 4085-4097.

Chapters

16. Banks, M.S. & Backus, B.T. (1998) Use of horizontal disparity, vertical disparity, and eye position in slant perception. In L. Harris (ed.), *Vision and Action*. Oxford University Press.

Manuscripts under Review or in Preparation

17. Adams, W.J., Banks, M.S., & van Ee, R. (2001). Adaptation to three-dimensional distortions in human vision. *Nature Neuroscience*, in press.
18. James, F.M.K., Humphrey, G.K., Banks, M.S., & Vilis, T. (2001). Accurate slant judgements bsed on extra-retinal eye position, *Vision Research*, in press.
19. Hooge, I.T.C., Banks, M.S., & van den Berg, A.V. (2001). Subjective and objective measures of cyclovergence. *Vision Research*, in preparation.
20. Banks, M.S. Sibigtroth, M., & Backus, B.T. (2001). Perception of surface curvature from stereopsis. *Vision Research*, in preparation.
21. Sibigtroth, M. & Banks, M.S. (2001). The influence of otolith signals on heading judgments. *Vision Research*, in preparation.
22. Sibigtroth, M., Davidenko, N., & Banks, M.S. (2001). The influence of perspective signals on heading perception. *Vision Research*, in preparation.

6. Service for Air Force

During the grant period, the PI was asked to do a few things that might potentially benefit the Air Force.

In 1998, he traveled to Williams AFB in Arizona in order to meet with Byron Pierce and George Geri. During that trip, he consulted with Drs. Pierce and Geri on their ongoing research and discussed possible collaborations between the Berkeley and Williams' labs. This led to an equipment loan in which Williams sent us an SGI Crimson workstation and a Sony CRT projector.

In 2000, the PI was asked to join a team that would put together a research plan for the Spatial

Disorientation Program for the Air Force Research Labs. This work consisted of reviewing the previous research plans, evaluating a plan written by investigators at Wright-Patterson AFB, and then traveling to Brooks AFB for a two-day meeting chaired by Bill Ercoline. The outcome was a 5-year research plan that is currently being evaluated by the Air Force.

In 2000, the PI participated in the Civic Outreach Program for two days. He traveled to Moffett Airfield, Edwards AFB, Cheyenne Mountain, and Peterson AFB and participated in briefings, tours, and discussions with Air Force personnel.

In 2001, the PI traveled to Sweden to participate in a workshop with SAAB Military Aircraft Division. The workshop concerned visual problems encountered by aviators and possible solutions to the problems.

7. Significance of Research Program for Air Force

During this grant period, we examined visual navigation and space perception in humans. We believe that our research is highly relevant to the military aviation mission. The main area of Air Force need that is addressed by our research is spatial disorientation (SD) and the use of synthetic or enhanced visual display devices such as head-mounted displays (HMDs), night-vision goggles (NVGs), the advanced aircraft control station (ACS), and more.

SD remains a major safety problem in flight and SD is likely to become an even more serious problem as the next wave of aircraft (e.g., agile flight) is developed and put into flight. Our work on heading perception is aimed at determining the complex of visual and non-visual signals that are used to estimate the direction of self-motion and ones orientation with respect to gravity. Specifically, we are working on determining how much weight is given to various signals (e.g., optic flow vs vestibular) and how those weights depend on the viewing situation (e.g., weight given to vestibular increases as the optic flow information is degraded). With a better understanding of how the human nervous system computes and weights these various sources of information we will be able to provide the Air Force material relevant to pilot training, cockpit design, and the configuration of synthetic visual displays. Let us give one specific example. In our work on the somatogravic ("pitch up") illusion, we are trying to determine what visual cues must be present in order to override the vestibular-based illusion of upward pitch. Once we know what the critical visual cues are, we can recommend the design of an artificial cockpit display (e.g., an artificial horizon) that would minimize the illusion.

Our work on space perception, primarily slant and curvature perception and visual-haptic integration, is also quite relevant to the military aviation mission. In the next generation of military aircraft, we will see greater and greater reliance on synthetic visual displays. Indeed, if the closed cockpit (all virtual) aircraft is brought on line, all of the visual information provided to the pilot will be synthetic. We have found that perceived depth is based on the integration of numerous visual (e.g., disparity and texture gradient) and non-visual (e.g., eye muscle signals) cues. The final percept is the result of a weighted combination of those various cues. An understanding of how those cues are calculated and weighted in the nervous system is critical to the design of a synthetic visual display. For example, we know from our work that cues provided by the CRT itself (e.g., pixelization, focus cues) cause perceptual depth compression. Such compression would be highly undesirable in an all-virtual cockpit and so the design of the visual display will either have to reduce the influence of such competing cues or figure out how to override them.

Finally, our software development might also be quite useful to the Air Force. At a meeting at Brooks AFB in March, 2000 (chaired by Bill Ercoline), a potential business plan was formed for the next 5 years. One idea presented in this plan was to generate web-based instructional aides for teaching spatial disorientation to future pilots. One of our software developments – FlightTools – would allow us to recreate flight scenarios that could be played on the internet for use in the classroom. Those scenarios could be seen from the perspective of the pilot or from an outside perspective (chosen by the student). The scenarios can be produced on standard PCs with off-the-shelf video cards. The Banks Lab is committed through its relationship with the Air Force to produce material like this whenever it might be needed.

8. Literature Cited

Backus, B.T. & Banks, M.S. (1999). Estimator reliability and distance scaling in stereoscopic slant perception. *Perception*, **28**, 217-242.

Backus, B.T., Banks, M.S., van Ee, R. & Crowell, J.A. (1999). Horizontal and vertical disparity, eye position, and stereoscopic slant perception. *Vision Research*, **39**, 1143-1170.

Banks, M.S. & Backus, B.T. (1998a). Extra-retinal and perspective cues cause the small range of the induced effect. *Vision Research*, **38**, 187-194.

Banks, M.S. & Backus, B.T. (1998b) Use of horizontal disparity, vertical disparity, and eye position in slant perception. In L. Harris (ed.), *Vision and Action.* Oxford University Press.

Banks, M.S., Backus, B.T., & Banks, R.S. (2001). Is vertical disparity used to estimate azimuth? *Vision Research,* in press.

Banks, M.S., Ehrlich, S.M., Backus, B.T., & Crowell, J.A. (1996). Estimating heading during real and simulated eye movements. *Vision Research,* **36**, 431-443.

Banks, M.S., Hooge, I.T.C., & Backus, B.T. (2001). Perceiving slant about a horizontal axis from stereopsis. *Journal of Vision,* **1**, 55-79.

Brookes, A. & Stevens, K.A. (1989). The analogy between stereo depth and brightness. *Perception,* **18**, 601-614.

Buckley, D. & Frisby, J. P. (1993). Interaction of stereo, texture and outline cues in the shape perception of three-dimensional ridges. *Vision Research,* **33**, 919-33.

Clarke, J. J. & Yuille, A.L. (1990). *Data Fusion for Sensory Information Processing Systems.* Boston : Kluwer.

Crowell, J. A., Banks, M.S., Shenoy, K.V., & Andersen, R.A. (1998). Visual self-motion perception during head turns. *Nature Neuroscience,* **1**, 732-737.

Cumming, B. G., Johnston, E. B., & Parker, A. J. (1993). Effects of different texture cues on curved surfaces viewed stereoscopically. *Vision Research,* **33**, 827-38.

Cutting, J. E. & Millard, R. T. (1984). Three gradients and the perception of flat and curved surfaces. *Journal of Experimental Psychology: General,* **113**, 198-216.

Ehrlich, S.M., Beck, D.M., Crowell, J.A., Freeman, T.C.A., & Banks, M.S. (1998). Depth information and perceived self-motion during simulated gaze rotations. *Vision Research,* **38**, 3129-3145.

Ernst, M.O., Banks, M.S., & Bültholff, H.H. (2000) Touch can change visual slant perception. *Nature Neuroscience,* **3**, 69-73.

Ernst, M.O. & Banks, M.S. (2001) Human combine visual and haptic information in a statistically optimal fashion. *Nature,* in press.

Fahle, M. & Westheimer, G. (1988). Local and global factors in disparity detection of rows of points. *Vision Research,* **28**, 171-178.

Foley, J.M. (1980). Binocular distance perception. *Psychological Review,* **87**, 411–34.

Freeman, T.C.A. (1999). Path perception and Filehne illusion compared: model and data. *Vision Research,* **39**, 2659-2667.

Freeman, T.C.A. & Banks, M. S. (1998). Perceived head-centric speed is affected by both extra-retinal and retinal errors. *Vision Research,* **38**, 941-945.

Freeman, T.C.A., Crowell, J.A., & Banks, M.S. (2000). Errors in path perception during gaze rotation. *Perception & Psychophysics,* **62**, 900-909.

Gårding, J., Porrill, J., Mayhew, J.E., & Frisby, J.P. (1995). Stereopsis, vertical disparity and relief transformations. *Vision Research,* **35**, 703-722.

Gharamani, Z., Wolpert, D.M., & Jordan, M.I. (1997). In *Self-organization, computational maps, and motor control.* (eds Morasso, P.G. & Sanguineti, V.), Amsterdam: Elsevier.

Gibson, J.J. (1950). *The perception of the visual world.* Boston: Houghton-Mifflin.

Gibson, J.J., Olum, P., & Rosenblatt, F. (1955). Parallax and perspective during aircraft landings. *American Journal of Psychology,* **68**, 373-385.

Gillam, B. & Lawergren, B. (1983). The induced effect, vertical disparity, and stereoscopic theory. *Perception and Psychophysics,* **34**, 121–30.

Gillam, B. & Ryan, C. (1992). Perspective, orientation disparity, and anisotropy in stereoscopic slant perception. *Perception,* **21**, 427-39.

Gillam, B., Chambers, D., & Lawergren, B. (1988). The role of vertical disparity in the scaling of stereoscopic depth perception: An empirical and theoretical study. *Perception and Psychophysics,* **40**, 477–83.

Gogel, W.C. (1956). The tendency to see objects as equidistant and its inverse relation to lateral separation. *Psychological Monographs,* **70**, 1-17.

Graham, M.E. & Rogers, B.J. (1982). Simultaneous and successive contrast effects in the perception of depth from motion-parallax and stereoscopic information. *Perception,* **11**, 247-262.

Harker, G.S. (1962). Apparent frontoparallel plane, stereoscopic correspondence, and induced cyclorotation of the eyes. *Perceptual and Motor Skills,* **14**, 75-87.

Harris, C.S. (1980). Perceptual adaptation to inverted, reversed, and displaced vision. *Psychological Reviews,* **72**, 419-444.

Heller, L. M. & Trahiotis, C. (1996) Extents of laterality and binaural interference effects. *Journal of the Acoustical Society of America,* **99**, 3632-3637.

Hooge, I.T.C., Banks, M.S., & van den Berg, A.V. (2000). Subjective and objective measures of cyclovergence. *Vision Research,* in preparation.

Howard, I. P. & Kaneko, H. (1994). Relative shear disparities and the perception of surface inclination. *Vision Research,* **34**, 2505-17.

Howard, I. P. & Rogers, B.J. (1995). *Binocular vision and stereopsis.* New York: Oxford Press.

Howard, I.P., Ohmi, M., & Sun, L. (1993). Cyclovergence: A comparison of objective and psychophysical measurements. *Experimental Brain Research*, **97**, 349-355.

Howard, I.P. (1982). *Human spatial orientation.* Chichester: Wiley.

James, F.M.K., Humphrey, G.K., Banks, M.S., & Vilis, T. (2001). Accurate slant judgements based on extra-retinal eye position. *Vision Research*, in press.

Kaneko, H. & Howard, I. P. (1996). Relative size disparities and the perception of surface slant. *Vision Research*, **36**, 1919-1930.

Knill, D.C. (1998). Discrimination of planar surface slant from texture: Human and ideal observers compared. *Vision Research*, **38**, 1683-1697.

Koenderink, J. J. & van Doorn, A. J. (1976). Geometry of binocular vision and a model for stereopsis. *Biological Cybernetics*, **21**, 29–35.

Landy, M. S., Maloney, L. T., Johnston, E. B. & Young, M. (1995). Measurement and modeling of depth cue combination: in defense of weak fusion. *Vision Research*, **35**, 389-412.

Longuet–Higgins, H. C. (1982). The role of the vertical dimension in stereoscopic vision. *Perception*, **11**, 371–6.

Mack, A. & Herman, E. (1973). Position constancy during pursuit eye movements: an investigation of the Filehne illusion. *Journal of Experimental Psychology*, **25**, 71-84.

Mack, A. & Herman, E. (1978). The loss of position constancy during pursuit eye movements. *Vision Research*, **18**, 55-62.

Mayhew, J. E. W. & Longuet–Higgins, H. C. (1982). A computational model of binocular depth perception. *Nature*, **297**, 376–8.

Mitchison, G. J. and McKee, S. P. (1990). Mechanisms underlying the anisotropy of stereoscopic tilt perception. *Vision Research*, **30**, 1781–91.

Nakayama, K. & Balliet, R. (1977). Listing's Law, eye position sense, and perception of the vertical. *Vision Research*, **27**, 453-457.

Nelson, J. (1977). The plasticity of correspondence: after-effects, illusions and horopter shifts in depth perception. *Journal of Theoretical Biology*, **66**, 203-266.

Ogle, K.N. (1938). Induced size effect. I. A new phenomenon in binocular space–perception associated with the relative sizes of the images of the two eyes. *AMA Archives of Ophthalmology*, **20**, 604–23.

Ogle, K.N. (1946). The binocular depth contrast phenomenon. *American Journal of Psychology*, **59**, 111-126.

Ogle, K.N. (1950). *Researches in binocular vision*. Hafner, New York.

Ogle, K.N. & Ellerbrock (1946).

Pastore, N. & Terwilliger, M. (1966). Induction of stereoscopic depth effects. *British Journal of Psychology*, **57**, 201-202.

Pastore, N. (1964). Induction of stereoscopic depth effect. *Science*, **144**, 888.

Pierce, B.J., Howard, I.P., & Feresin, C. (1998). Depth interactions between inclined and slanted surfaces in vertical and horizontal orientations. *Perception*, **27**, 87-103.

Poggio, T., Gamble, E.B., & Little, J.J. (1998). Parallel integration of vision modules. *Science*, **242**, 436-439.

Power, R.P. (1980). The dominance of touch by vision: sometimes incomplete. *Perception*, **9**, 457-466.

Rock, I. & Victor, J. (1964). Vision and touch: An experimentally created conflict between the two senses. *Science*, **143**, 594-596.

Rogers, B.J. (1992). The perception and representation of depth and slant in stereoscopic surfaces. (In G.A. Orban & H.H. Nagel, eds), *Artificial and biological vision systems.* Berlin: Springer.

Rogers, B.J. & Bradshaw, M.F. (1993). Vertical disparities, differential perspective and binocular stereopsis. *Nature*, **361**, 253–255.

Rogers, B. J. & Bradshaw, M. (1995). Disparity scaling and the perception of frontoparallel surfaces. *Perception*, **24**, 155-179.

Rogers, B. J. & Graham, M. E. (1983). Anisotropies in the perception of three–dimensional surfaces. *Science*, **221**, 1409–1411.

Royden, C.S., Banks, M.S., & Crowell, J.A. (1992). The perception of heading during eye movements. *Nature*, **360**, 583-585.

Royden, C.S., Crowell, J.A., & Banks, M.S. (1994). Estimating heading during eye movements. *Vision Research*, **34**, 3197-3214.

Royden, C.S. (1994). Analysis of misperceived observer motion during simulated eye rotations. *Vision Research*, **34**, 3215-3222.

Sedgwick, H. A. (1986). Space perception. *In Handbook of human perception and performance*, (ed. K. R. Boff, L Kaufman, & J. P. Thomas), Chap. 21. Wiley, New York.

Sibigtroth, M.P. & Banks, M.S. (2000). Perspective transformation in heading estimation. *ARVO* presentation.

Sibigtroth, M.P. & Banks, M.S. (2001). Visual-vestibular interactions in heading perception. *VSS* presentation.

Somani, R.A., DeSouza, J.F., Tweed, D., & Vilis, T. (1998). Visual test of Listing's law during vergence. *Vision Research*, **38**, 911-923.

Stevens, K.A. & Brookes, A. (1988). Integrating stereopsis with monocular interpretations of planar surfaces. *Vision Research*, **28**, 371-386.

van den Berg, A.V. & Brenner, E. (1994). Humans combine the optic flow with static depth cues for robust perception of heading. *Vision Research*,**34**, 2153-2167.

van den Berg, A.V. (1996). Judgments of heading. *Vision Research*, **36**, 2237-2350.

van Ee, R. & Erkelens, C. J. (1996). Anisotropy in Werner's binocular depth contrast effect. *Vision Research*, **36**, 2253-2262.

van Ee, R., Banks, M. S., & Backus, B. T. (1999). An analysis of binocular slant contrast. *Perception*, **28**, 1121-1145.

van Ee, R. (1995). *Stability of binocular depth perception.* Utrecht: Utrecht University.

Warren, W.H., Morris, M.W., & Kalish, M. (1988). Perception of translational heading from optical flow. *Journal of Experimental Psychology*, **17**, 28-43.

Welch, R.B. (1986). *Perceptual modification: Adapting to altered sensory environments.* New York: Academic.

Werner, H. (1937). Dynamical theory of depth perception. *Psychological Monographs*, **49**, 1-127.

Werner, H. (1938). Binocular depth-contrsadt and the conditions of the binocular field. *American Journal of Psychology*, **51**, 489-497.

Wertheim, A.H. (1987). Motion perception during self-motion-the direct versus inferential controversy revisited. *Behavioural and Brain Sciences*, **17**, 293-311.

Yasui, S. & Young, L.R. (1975). Perceived visual motion as effective stimulus to pursuit eye movement system. *Science*, **190**, 906-908.